IJMMM International Journal of Minerals, Metallurgy and Materials 矿物冶金与材料学报（英文版）

Mechanical properties, deformation response, energy evolution, and failure pattern of stratified cemented tailings backfill under triaxial compression

Wenbin Xu, Yalun Zhang, Kangqi Zhao, and Tong Sun

Cite this article as:
Wenbin Xu, Yalun Zhang, Kangqi Zhao, and Tong Sun, Mechanical properties, deformation response, energy evolution, and failure pattern of stratified cemented tailings backfill under triaxial compression, *Int. J. Miner. Metall. Mater.*, (2025). https://doi.org/10.1007/s12613-025-3102-1

View the article online at SpringerLink or IJMMM Webpage.

INTERNATIONAL JOURNAL OF
Minerals, Metallurgy and Materials

Research Article https://doi.org/10.1007/s12613-025-3102-1

Mechanical properties, deformation response, energy evolution, and failure pattern of stratified cemented tailings backfill under triaxial compression

Wenbin Xu✉, *Yalun Zhang*, *Kangqi Zhao*, *and Tong Sun*

School of Energy and Mining Engineering, China University of Mining & Technology (Beijing), Beijing 100083, China
(Received: 23 October 2024; revised: 20 January 2025; accepted: 27 January 2025)

Abstract: The backfill should keep stable in the primary stope when mining an adjacent secondary stope in subsequent open stoping mining methods, and the large-size mined-out area is usually backfilled by multiple backfilling before the recovery of a secondary stope, resulting in a layered structure of backfill in stope. Therefore, it is significant to investigate the deformation responses and mechanical properties of stratified cemented tailings backfill (SCTB) with different layer structures to remain self-standing as an artificial pillar in the primary stope. The current work examined the effects of enhance layer position (1/3, 1/2, and 2/3) and thickness ratio (0, 0.1, 0.2, and 0.3) on the mechanical properties, deformation, energy evolution, microstructures, and failure modes of SCTB. The results demonstrate that the incorporation of an enhance layer significantly strengthens the deformation and strength of SCTB. Under a confining pressure of 50 kPa, the peak deviatoric stress rises from 525.6 to 560.3, 597.1, and 790.5 kPa as the thickness ratio of enhance layer is increased from 0 to 0.1, 0.2 and 0.3, representing a significant increase of 6.6%, 13.6% and 50.4%. As the confining pressure increases, the slopes of the curves in the elastic stage become steep, and the plastic phase is extended accordingly. Additionally, the incorporation of the enhance layer significantly improves the energy storage linit of SCTB specimen. As the thickness ratio of the enhance layer increases from 0 to 0.1, 0.2, and 0.3, the elastic energy rises from 0.54 to 0.67, 0.84, and 1.00 MJ·m^{-3}, representing a significant increase of 24.1%, 55.6% and 85.2%. The internal friction angles and cohesions of the SCTB specimens are higher than those of the CTB specimens, however, the cohesion is more susceptible to enhance layer position and thickness ratio than the internal friction angle. The failure style of the SCTB specimen changes from shear failure to splitting bulging failure and shear bulging failure with the presence of an enhance layer. The crack propagation path is significantly blocked by the enhance layer. The findings are of great significance to the application and stability of the SCTB in subsequent stoping backfilling mines.

Keywords: stratified cemented tailings backfill; enhance layer; triaxial compressive tests; mechanical properties; energy evolution

1. Introduction

The rapid growth of the mining sector has spurred remarkable economic development in numerous nations. However, this mineral extraction, notably of metallic resources, has also posed numerous challenges, including the management of solid waste and the handling of voids left by underground mining activities [1–3]. Solid wastes (such as tailings and waste rock) not only occupy a large amount of land resources but also contain harmful substances in some untreated or improperly treated tailings, which pose a serious effect on the environment [4–5]. In addition, the underground goafs may induce rock bursts and subsidence hazards. At present, a novel mining technology, cemented tailings backfill (CTB), is adopted in an increasing number of mines around the world. It is commonly composed of cementitious materials, tailings, water, and other mineral or chemical admixtures, which are usually transported into underground goafs or stopes by gravity flow or pump. The CTB not only eliminates the potential collapse hazards but also disposes of a large number of tailings. Therefore, it has become one of the eco-friendly and safe mining technologies lately [6–7]. The mechanical strength of CTB is crucial for maintaining the stability of the primary stope as mining an adjacent secondary stope in subsequent open stoping mining method, which is mainly gained by hydration reaction from cementitious materials with water. Consequently, the binder cost of CTB accounts for approximately 70% of the total backfill operation costs [8–10]. Many ways have been employed to improve the strength and decrease the costs of CTB. The mechanical property of CTB is mainly influenced by a combination of external and internal factors, such as cement-to-tailings ratio (c/t), mass concentration, temperature, curing time, and other mineral admixtures. Research by Xu *et al*. [11–12] demonstrated that low temperatures impede the strength development of CTB, whereas higher temperatures lead to enhanced strength. Jin *et al*. [13] investigated the effects of different particle sizes of tailings on the strength of the CTB. It was observed that as the particle size of the tailings increased, the strength and elastic modulus of the CTB first increased

✉ Corresponding author: Wenbin Xu E-mail: xuwb08@163.com

and then decreased. Jssem and Xu [14], and Xu *et al*. [15] also found that the silica fume can improve the strength of CTB. The above research has made important progress in understanding the way to increase the mechanical properties of CTB.

In practice, the distinctive backfilling sequence is commonly used to save the backfill cost in traditional subsequent open stoping mining, that is to say, the top layer and bottom layer are backfilled with a high concentration of cement, while the middle layer utilizes a lower concentration of cement [16–18], as shown in Fig. 1. However, as a result of the reduced strength in the middle layer of CTB, it is vulnerable to disturbances caused by mining in neighboring stope, which significantly influences the stability of the primary stope in a subsequent stage of mining [19–21]. Wang *et al*. [22] explored how the cement-to-tailings ratio and the thickness of the middle layer impact the strength of layered cemented tailings backfill (LCTB). The strength of the CTB rises as the thickness of the middle layer decreases and the c/t ratio increases. Research by Zhang *et al*. [23] indicated that both the peak strength and the elastic modulus of LCTB samples are enhanced by reducing the number of layers and by applying higher confining pressure. According to Wang *et al*. [24], the unconfined compressive strength (UCS) of LCTB decreased with increasing height of middle layer and decreasing cement-to-tailings ratio. Research has verified that the development of strength and the mode of failure in SCTB is predominantly influenced by factors such as the number of layers, the cement-to-tailings ratio, and the number of intermediate layers [25–27]. Yet, no viable strategies have been proposed to strengthen the mechanical characteristics of the middle layer, which remains the weakest part of the SCTB in actual mine stopes [28–29]. A solid knowledge of the strength evolution and failure mode of the SCTB is crucial for stability analysis and backfill design of CTB in subsequent open stoping mining methods.

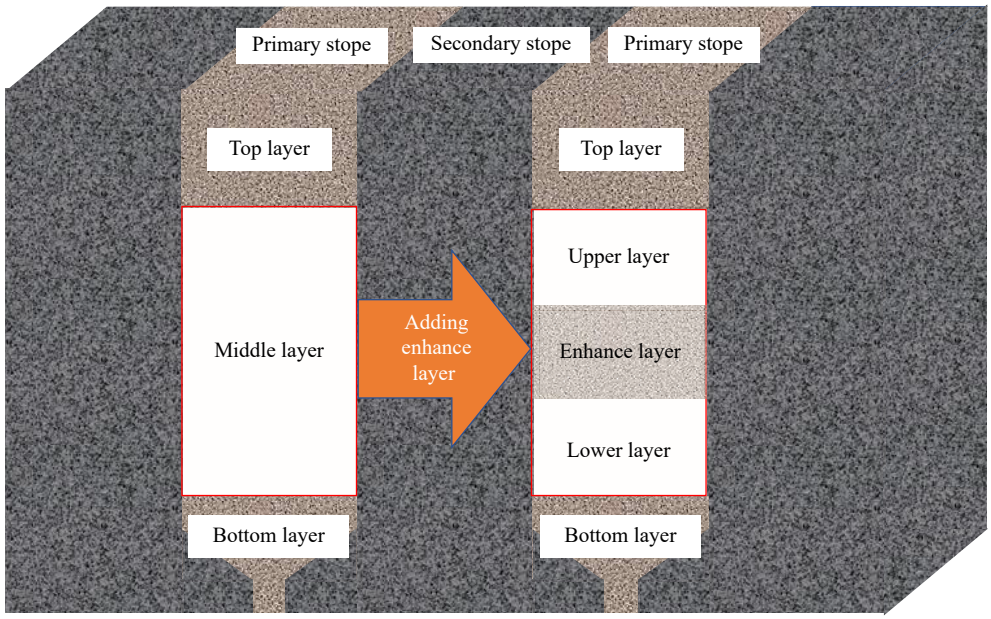

Fig. 1. Sketch of stratified cemented tailings backfill.

In underground environments, the cemented tailings backfill are generally under triaxial stress conditions. Many scholars have studied the triaxial mechanical properties of cemented tailings backfill [30–32]. Zhang *et al*. [23] studied the effects of the layer number and confining pressure on the mechanical properties of layered cemented tailings backfill (LCTB) samples. Yu *et al*. [33] studied the triaxial mechanical properties and failure modes of rock-backfill composite specimens, and investigated the evolution of the interface between rock and CTB through Computed tomography scanning. Wang *et al*. [34] conducted triaxial compression tests and microstructural tests to study the effects of the number of dry-wet cycle state transitions on the triaxial mechanical properties of solid waste cemented backfilling samples, and established a constitutive model to reflect the stress state and failure process of the specimens. Xu *et al*. [35] investigated the influence of the confining pressure, curing age, and cement content on the development of hydraulic conductivity. The above research mainly focuses on investigating the triaxial mechanical properties of intact CTB specimens and conventional structural cemented tailings backfill. However, few researches have been conducted to investigate the triaxial compressive property of stratified cemented tailings backfill (SCTB) with enhance layer.

This study introduces a novel approach to optimizing the mechanical properties of SCTB, as shown in Fig.1. In this method, the middle layer is backfilled with lower cement content, compared with the bottom and top layers. The enhance layer is desired to prevent backfill collapse in the primary stope due to mining secondary stope. In this study, the triaxial compressive responses of CTB specimens with different enhance layer positions and thickness ratios are characterized using the triaxial compressive apparatus. The testing results for SCTB with enhance layer are presented, in-

cluding the mechanical property, deformation behavior, energy dissipation evolution, and failure mode under triaxial compression. The main objective of this study is to improve the mechanical property of SCTB to meet the backfilling requirements under various mining conditions, while reducing material cost and environmental impact. The conclusions are greatly significant for guaranteeing the successful application and stability of SCTB in subsequent stoping backfilling operation.

2. Experimental

2.1. Materials

The SCTB samples were prepared using silica tailings (ST), which primarily contain 99.6wt% of silicon dioxide. The grain size distribution of ST is illustrated in Fig. 2. Over 30wt% of the material consists of fine particles, preventing the separation of the fresh CTB mixture. The preparation of fresh SCTB involves the use of Ordinary Portland Cement (OPC, P.O. 42.5R). Table 1 provides a breakdown of the primary chemical components of OPC. Additionally, apart from the components listed in the Table 1, the content of loss on ignition (LOI) is 2.75wt%. A mixture of cement and ST was prepared using tap water.

2.2. Mix proportions and specimen preparation

The cement content of CTB in stope is mixed at a cement-to-tailings ratio of 1:20, and thus the upper and lower layers

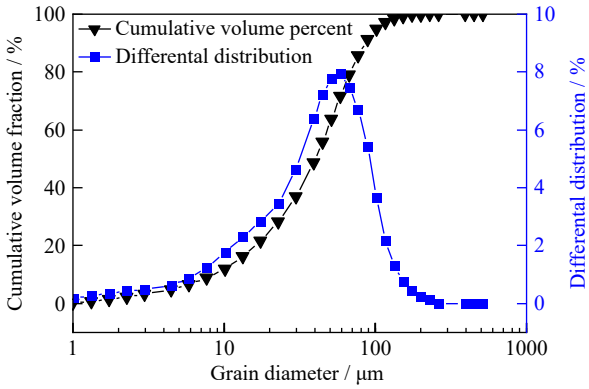

Fig. 2. Grain size distribution of used ST.

Table 1. Chemical components of the cement wt%

CaO	SiO_2	Fe_2O_3	Al_2O_3	K_2O	MgO	SO_3	Na_2O	TiO_2
64.78	20.34	3.11	5.02	0.35	1.09	2.20	0.10	0.26

in SCTB specimens are designed as a cement-to-tailings ratio of 1:20. The cement content of the enhance layer in SCTB is designed at 1:10. The detailed experimental propose and parameters of SCTB specimens are presented in Fig. 3 and Table 2. In Fig. 3, H represents the height of both CTB and SCTB specimen. Where h is the thickness of the enhance layer. The thickness ratio of the enhance layer is defined as the ratio of the enhance layer thickness to the total specimen height (h/H). Where p is the vertical distance from the midpoint of the enhance layer thickness to the bottom of the specimen. The position of the enhance layer is defined as the ratio of the p-value to the total specimen height (p/H).The enhance layer positions are located at 1/3, 1/2, and 2/3 of the CTB specimens, respectively, and the thickness ratio of the enhance layer is set as 0.1, 0.2, and 0.3. The confining pressure is set as 0, 50, 100, 150, and 200 kPa, which maintains consistency with the selection of confining pressures in previous studies and standards [36].

The tailings, cement, and tap water were fully mixed with an agitator for more than 5 min. Once thoroughly mixed, the fresh mixture was transferred into cylindrical molds with dimensions of 50 mm in diameter and 100 mm in height. In the course of layering, the mixture was compacted using a stirrer rod to minimize air pockets, thereby enhancing the likelihood of successful specimen fabrication. Subsequently, the SCTB specimens were allowed to cure in a curing chamber, where the humidity was maintained within a range of 95% ± 5% and the temperature was kept at 20°C ± 5°C. In practice, the backfill in primary stope is usually exposed for a curing period of more than 28 d to gain enough strength through binder hydration and drainage. Therefore, the curing time for SCTB specimens is set to 28 d.

2.3. Test apparatus and procedure

2.3.1. Triaxial compressive strength testing

The triaxial compressive tests were performed on SCTB specimens after 28 d of curing in accordance with ASTM

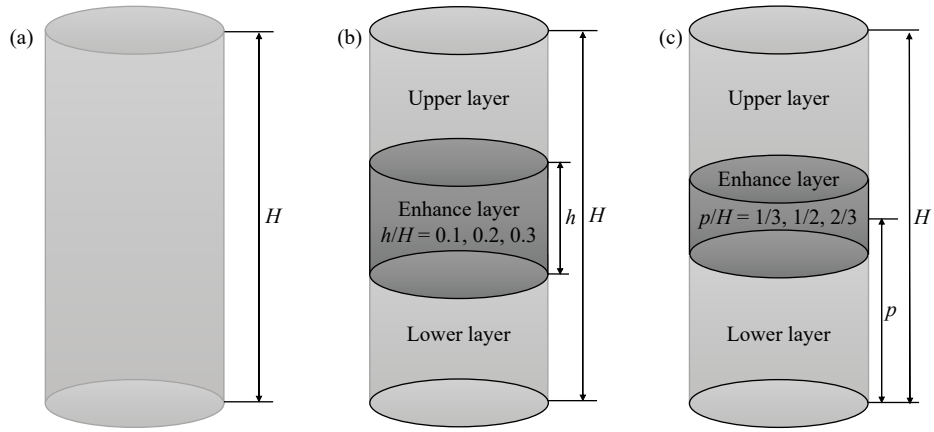

Fig. 3. Schematic diagram of SCTB specimen: (a) CTB; (b) thickness ratio of enhance layer; (c) position of enhance layer.

Table 2. Mix proportions for SCTB specimens

Cement-to-tailings ratio of upper and lower layers	Cement-to-tailings ratio of enhance layer	Position of enhance layer	Thickness ratio of enhance layer
1:20			0
1:20	1:10	1/3	0.2
1:20	1:10	1/2	0.2
1:20	1:10	2/3	0.2
1:20	1:10	1/2	0.1
1:20	1:10	1/2	0.3

D4767–11 [37]. The desired SCTB specimens were installed between two porous stone caps. The samples were surrounded by a latex membrane. The pressing apparatus, with a loading capacity of 60 kN, and a confining pressure ranging from 0 to 2 MPa was commanded by a computer. Each specimen was loaded at a deformation rate of 0.5 mm·min^{-1} during testing. A set of confining pressures used for each group of SCTB specimens were designed at 0, 50, 100, 150, and 200 kPa, respectively.

2.3.2. Microstructural analysis

To better investigate the effect of enhance layer on the mechanical properties of SCTB samples, microstructural analysis including mercury intrusion porosimeter (MIP) testing and scanning electron microscopy (SEM) were conducted on the desired SCTB specimens. SEM was used to examine the crystal structure, distribution, and morphology of hydrated products in SCTB specimens by a Quanta 250 FEG device. Additionally, the pore size distribution of enhance layer in SCTB specimen was also monitored using Auto Pore IV 9520.

3. Results and discussion

3.1. Effect of enhance layer position on the triaxial compressive property of SCTB

The deviatoric stress versus axial strain and volumetric strain curves of SCTB specimens with different enhance layer positions (1/3, 1/2, and 2/3) under different confining pressures (0, 50, 100, 150, and 200 kPa) are shown in Fig. 4, respectively, where V and ε_1 represent the volumetric strain and axial strain of the specimen, respectively. For instance, V-50 kPa means the deviatoric stress versus volumetric strain curve of the specimens under a confining pressure of 50 kPa. ε_1-50 kPa means the deviatoric stress versus axial strain curve of the specimen under a confining pressure of 50 kPa. It can be seen from Fig. 4 that the deviatoric stress shows a linear growth with axial strain at the beginning of stress and strain curves for all the SCTB samples, then the deviatoric stress

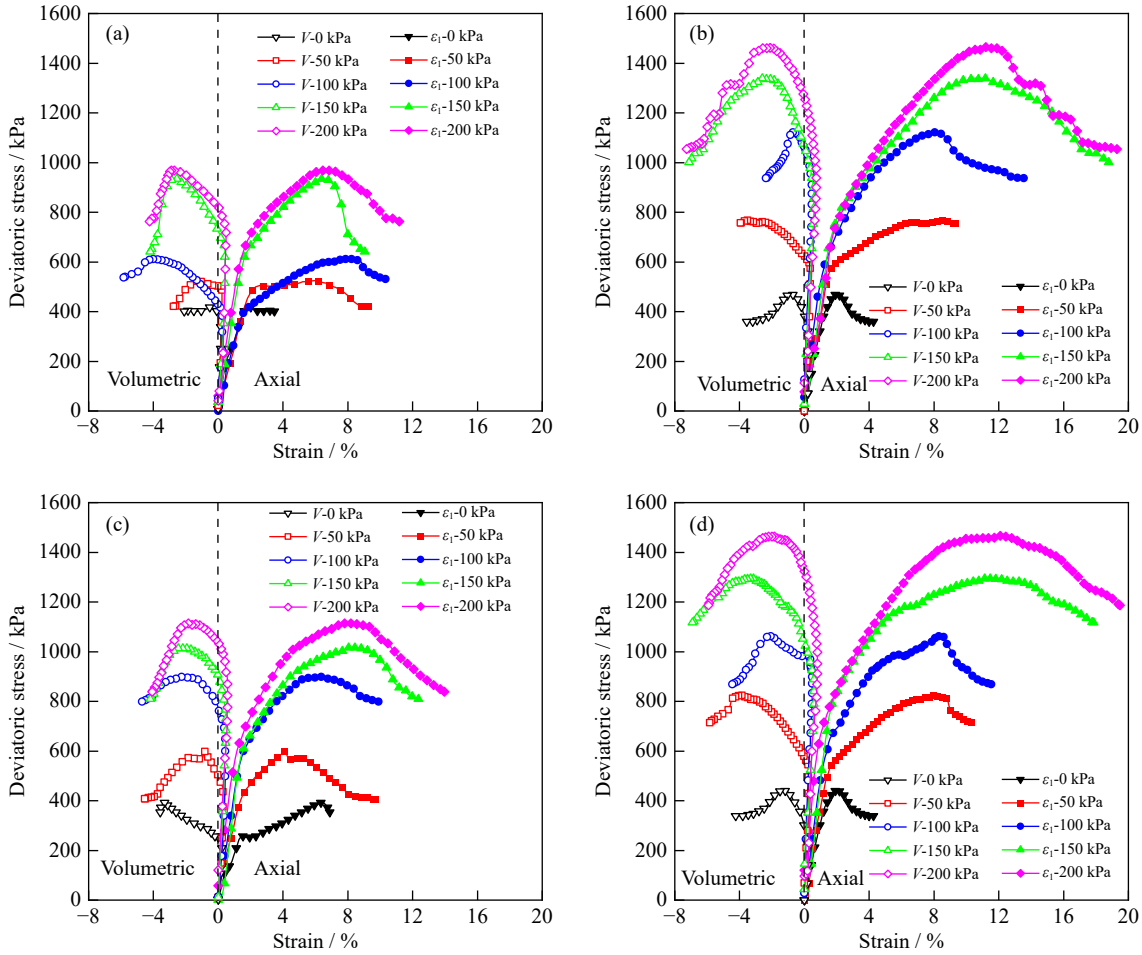

Fig. 4. Deviatoric stress–strain and deviatoric stress–volumetric strain curves of SCTB samples with different enhance layer positions: (a) CTB without enhance layer; (b) enhance layer position of 1/3; (c) enhance layer position of 1/2; (d) enhance layer position of 2/3.

gradually increases to plateau strength as strain increases and subsequently presents a gentle reduction in strength. Moreover, with the confining pressures increase, the slope of the curve becomes steeper, and the peak deviatoric stress and axial strain at failure of the SCTB specimen increase as well, irrespectively of enhance layer position. It is also shown in Fig. 4 that the plastic response of SCTB with enhance layer becomes prominent compared with the CTB without enhance layer, and the plastic phase is extended accordingly. In addition, the strain-hardening after the post-peak stress–strain curve induced by the enhance layer is more pronounced than the CTB. It means that the stress–strain response of the SCTB specimen is strengthened by the enhance layer.

Fig. 4 also presents the deviatoric stress and volumetric strain values of SCTB specimens with different enhance layer positions under different confining pressures as well. It is worth noting that for volumetric strain, negative values represent dilative expansion and positive values represent compression. It can be seen from Fig. 4 that the volumetric strain values of SCTB specimens display contractive behavior at the beginning of the compression stage, as the axial strain increases, the deformation behavior turns into expansion. The volumetric strain is firstly related to the compaction degree of tailings particle and the interlayer pore in SCTB specimen. In this stage, the initial pores and fissures in SCTB specimens are compressed and some tiny cracks are generated. At this point, the expansive deformation of the SCTB sample is smaller than the axial compressive deformation, leading to an increase in volumetric strain, the conclusion is also verified by other researchers [38–40]. As the axial loading increases to a certain value, when the axial deformation is equal to the transverse deformation, the volumetric strain keeps a constant value with increasing axial loading. This stage is defined as the critical stage of triaxial compressive deformation, which is the transition from contractive to dilative. With the increase of the axial loading, the transverse deformation is larger than the axial deformation, leading to the volume expansion at higher axial loading.

In addition, the maximum compression in the volumetric strain of SCTB sample varies with the position of enhance layer and confining pressure. The maximum compression in the volumetric strain of SCTB sample is listed in Table 3. As shown in Table 3, the maximum compression in the volumetric strain of SCTB specimen increases with the confining pressure. It is mainly due to higher confining pressure inhibits the transverse deformation [41]. Moreover, the maximum compression of SCTB specimen with an enhance layer is greater than that of CTB specimen. It is mainly supported that the enhance layer retards the lateral deformation of the upper and lower layer, leading to an increase in the maximum compression of volumetric strain. From Table 3, it can also be found that the maximum compression of the SCTB specimen with enhance layer at the position of 1/2 is smaller than that at the position of 1/3 and 2/3. This is consistent with the result of peak deviatoric stress.

To investigate the effect of enhance layer position on the

Table 3. Maximum compression in volumetric strain of different SCTB specimens

Position of enhance layer	Confining pressure / kPa	Maximum compression
0	50	0.24
	100	0.26
	150	0.42
	200	0.48
1/2	50	0.30
	100	0.44
	150	0.48
	200	0.57
1/3	50	0.37
	100	0.46
	150	0.59
	200	0.73
2/3	50	0.35
	100	0.48
	150	0.60
	200	0.80

Poisson's ratio of SCTB specimens, the Poisson's ratio of SCTB specimens with different enhance layer positions under different confining pressures is presented in Fig. 5. It can be concluded that the Poisson's ratio of SCTB with enhance layer is lower than that of CTB regardless of confining pressure. Additionally, the Poisson's ratio of the SCTB specimen with enhance layer at the position of 1/2 is higher than that at the position of 1/3 and 2/3. Furthermore, the Poisson's ratio of SCTB sample decreases with the increase of confining pressure when the position of enhance layer is fixed.

The peak deviatoric stress values of SCTB specimens with different enhance layer positions under different confining pressures are shown in Fig. 6. It can be concluded from Fig. 6 that the peak deviatoric stress values of SCTB specimens increase by enhance layer regardless of enhance layer position, the strengthening effect is magnified with increasing confining pressure. Furthermore, the peak deviatoric stress of the SCTB specimen with enhance layer at the position of 1/2 is smaller than that at the position of 1/3 and 2/3, but the peak deviatoric stress of SCTB is still higher than that of the CTB, except when the confining pressure is zero. Compared with

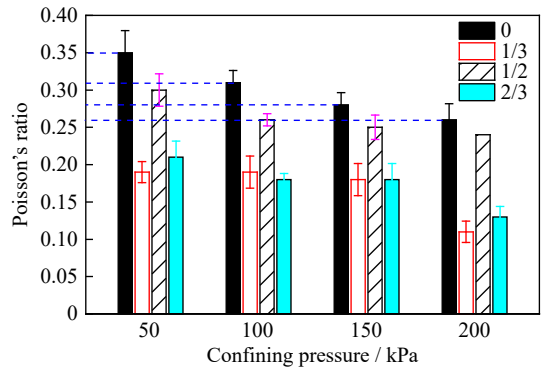

Fig. 5. Poisson's ratios of SCTB specimens with different enhance layer positions under different confining pressure.

CTB under confining pressure of 0, 50, 100, 150, and 200 kPa, the stress growth rate of SCTB with enhance layer at the position of 1/3 is increased by 11.9%, 51.9%, 83.2%, 43.3%, and 50.9%, respectively. It means that the compressive property is significantly strengthened by the enhance layer. It is noteworthy that, under a confining pressure of 0 kPa, the peak deviatoric stress of SCTB specimen with an enhance layer at the position of 1/2 is lower than that of CTB specimen. When the enhance layer is placed at the position of 1/2, it coincides with the region where the maximum tensile stress occurs during the triaxial compression test. The enhance layer, while providing some strength improvement, is not sufficient to fully counteract the high tensile stress in this critical region. Consequently, cracks are more likely to penetrate the enhance layer, leading to premature failure of the specimen and thus a lower peak deviatoric stress. In contrast, when the enhance layers is positioned at 1/3 or 2/3, it is located closer to the upper or lower of the specimen, where the tensile stress is relatively lower. The enhance layers in these positions can more effectively distribute the stress and provide additional strength to the weaker layers, delaying the onset of crack initiation and propagation. As a result, the specimen can withstand higher loads before failure occurs, leading to a higher peak deviatoric stress compared to the 1/2 position, as well as exceeding that of CTB specimen.

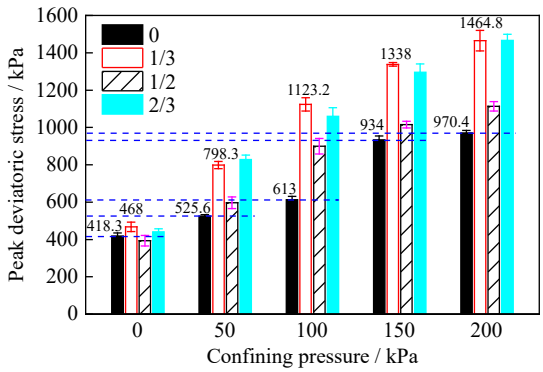

Fig. 6. Peak deviatoric stresses of SCTB samples with different enhance layer positions.

Fig. 7 illustrates the effect of enhance layer position on the internal friction angle and cohesion of SCTB specimens. It can be concluded that the internal friction angle and cohesion of the SCTB specimens are greater than those of the CTB specimens. The corresponding cohesion values of SCTB specimens with enhance layer positions of 1/2, 1/3, and 2/3 vary from 99.6 to 108.6, 129.8, and 131.9 kPa, respectively, and the internal friction angles change from 37.4° to 39.7°, 44.1° and 42.7°. It indicates that the cohesion is more susceptible to enhance layer than the internal friction angle. It is mainly attributed to that the internal friction angle of CTB is dominated by the tailing particles type and size [40].

3.2. Effect of enhance layer thickness ratio on the triaxial compressive property of SCTB

Preceding research has exposed that the mechanical properties of the SCTB are related to the thickness ratio of the

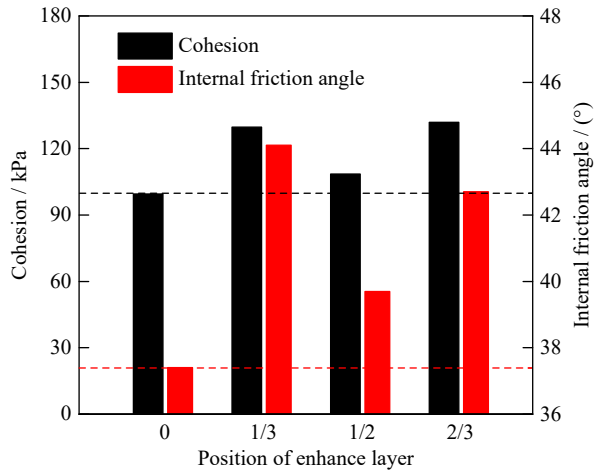

Fig. 7. Cohesion and internal friction angles of SCTB specimens at different enhance layer positions.

layer [42]. Therefore, the effect of the enhance layer thickness ratio on the SCTB specimen was studied. The deviatoric stress versus axial strain and volumetric strain curves of SCTB specimens with different thickness ratios of enhance layer (0.1, 0.2, and 0.3) under different confining pressures (0, 50, 100, 150, and 200 kPa) are shown in Fig. 8. It can be obtained that all deviatoric stress versus axial strain curves of the SCTB specimens show similar trends, which can be divided into three stages: the rapid increase phase of stress, the slow increase phase of stress and the stress decrease phase. Moreover, as the confining pressure increases, the extent of strain in the elastoplastic phase gradually increases. With the thickness ratio of the enhance layer increasing, the brittle characteristics of the specimen become more pronounced. As shown in Fig. 8(d), when the thickness ratio of the enhance layer is 0.3, the deviatoric stress reaches the peak and then rapidly decreases as the strain increases. The following discussions will focus on the influence of different enhance layer thickness ratios on the peak deviatoric stress, Poisson's ratio, elastic modulus, internal friction angle, and cohesion of the SCTB specimen.

The peak deviatoric stress values of SCTB specimens with different thickness ratios of enhance layer under triaxial compression are shown in Fig. 9. It is evident from Fig. 9 that the peak deviatoric stress values of SCTB specimens increase with the increase of enhance layer thickness ratio, regardless of confining pressure. For instance, under 50 kPa of confining pressure, the peak deviatoric stress rises from 525.6 to 560.3, 597.1, and 790.5 kPa as the thickness ratio of enhance layer is increased from 0 to 0.1, 0.2 and 0.3, representing a significant increase of 6.6%, 13.6% and 50.4%. The destruction and instability of SCTB specimen is attributed to the generation and propagation of interior crack. The interior cracks first arose in the low-strength region, and then gradually penetrated and expanded into the entire specimen, resulting in the overall instability of the specimen. The proportion of high-strength areas increases with the augmentation of the enhance layer thickness ratio, making it more difficult for cracks to propagate within the specimen, which results in an increase in overall strength.

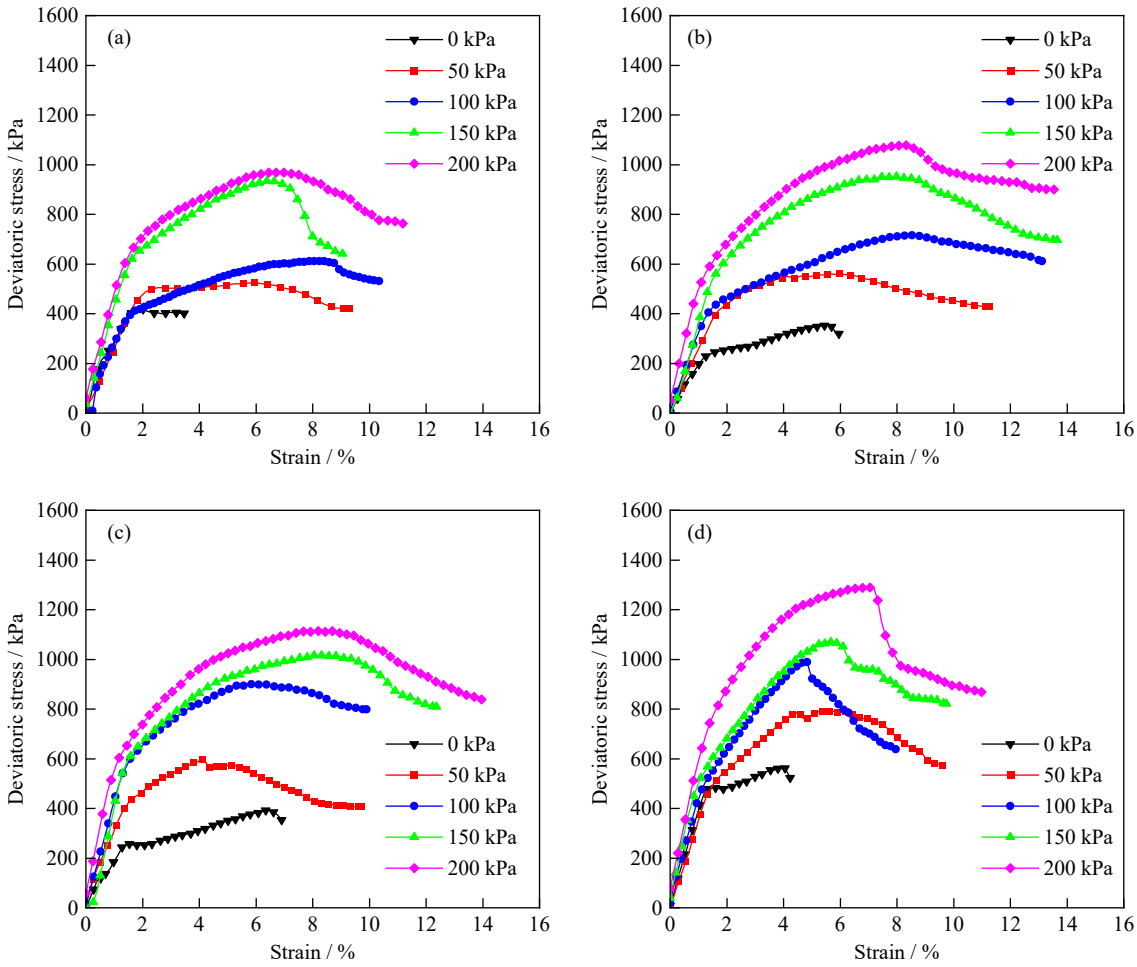

Fig. 8. Deviatoric stress–strain curves of SCTB samples with different enhance layer thickness ratios: (a) CTB without enhance layer; (b) thickness ratio of 0.1; (c) thickness ratio of 0.2; (d) thickness ratio of 0.3.

The stiffness, quantified by the elastic modulus, frequently serves to depict how SCTB samples resist deformation across different scenarios [43–44]. The elastic modulus of SCTB samples with different thickness ratios of enhance layer (0.1, 0.2, and 0.3) under different confining pressures (50, 100, 150, and 200 kPa) are shown in Fig. 10. As shown in Fig. 10, the elastic modulus of SCTB specimen increases observably with the thickness ratio of enhance layer. For instance, under a confining pressure of 100 kPa, the elastic modulus rises from 28 to 32.2, 41, and 43.9 MPa as the thickness ratio of enhance layer is increased from 0 to 0.1, 0.2 and 0.3, representing a significant increase of 15%, 46.4% and 56.8%. Except under a confining pressure of 0 kPa, the elastic modulus of SCTB specimen is larger than that of CTB specimen. It is mainly attributed to that the increase of the enhance layer thickness ratio is equivalent to increasing the hydration products in the SCTB specimen, which improves the overall cohesion of the SCTB specimen and thus enhances the elastic modulus [45]. When the confining pressure is 0 kPa, the elastic moduli of SCTB specimens with enhance layer thickness ratios of 0.1 and 0.2 are lower than those of CTB specimens. The stratified structure leads to an increase

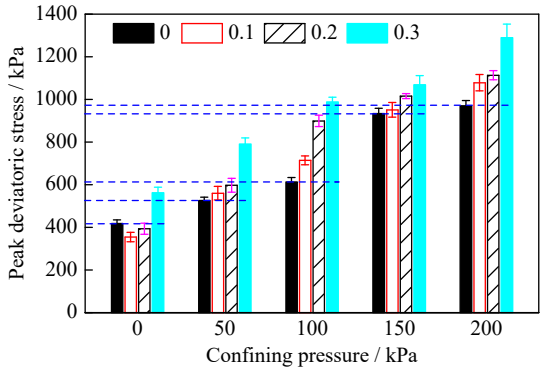

Fig. 9. Peak deviatoric stresses of SCTB specimens with different enhance layer thickness ratios.

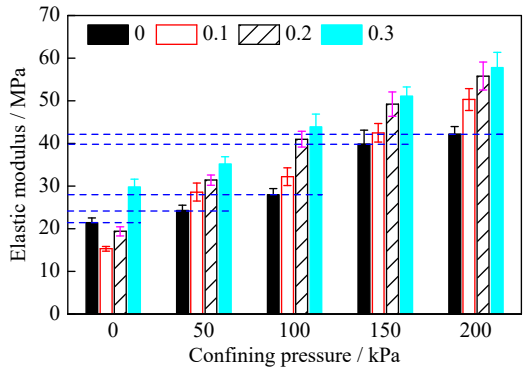

Fig. 10. Elastic moduli of SCTB specimens with different thickness ratios of enhance layer.

in internal defects within SCTB specimens. During the elastic deformation stage, these defects impede uniform deformation of the SCTB specimen, resulting in larger strains under smaller axial stresses and a reduction in the elastic modulus. As the thickness ratio of the enhance layer increases, the proportion of the high elastic modulus region expands, thereby enhancing the overall elastic modulus of SCTB specimens. When the thickness ratio of enhance layer increases to 0.3, the elastic modulus of SCTB specimen exceeds that of CTB specimen.

Fig. 11 illustrates the development in cohesion and internal friction angle of SCTB specimens with different enhance layer thickness ratios. The cohesion and internal friction angle of the SCTB specimen, which increase with the augmentation of the enhance layer thickness ratio, are both greater than those of CTB specimen. The corresponding cohesion value of the SCTB specimen with enhance layer thickness ratio of 0.1, 0.2, and 0.3 elevates from 99.6 to 102, 108.6, and 134.5 kPa, and the internal friction angle changes from 37.4° to 38.1°, 39.7° and 41.3°, respectively. It is evident that the cohesion significantly increases with the thickness ratio of enhance layer, while the increase in the internal friction angle is relatively limited. The increase in cohesion is primarily due to the enlargement of the hydration product volume within the SCTB specimen. However, the effect of hydration products on the internal friction angle is negligible. The results are also supported by previous research investigated by Xu *et al*. [40].

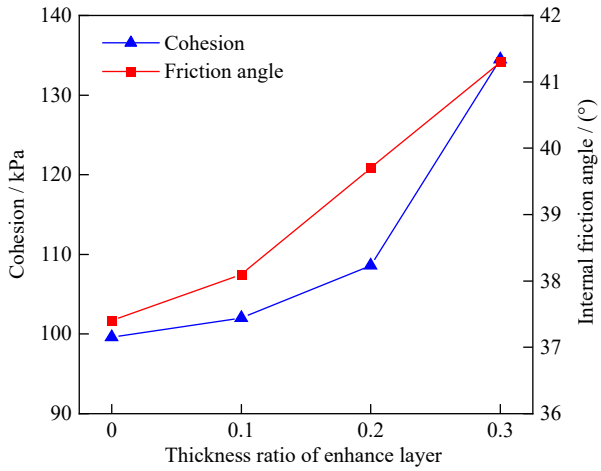

Fig. 11. Cohesions and internal friction angles of SCTB specimens with different enhance layer thickness ratios.

The variation curves of Poisson's ratios of SCTB specimens with different enhance layer thickness ratios under triaxial compression are shown in Fig. 12. As the Poisson's ratio of the SCTB with enhance layer is lower than that of CTB specimen, the Poisson's ratio of the SCTB specimen further decreases with the increase in the thickness ratio of enhance layer, regardless of the confining pressure. Meanwhile, the Poisson's ratio of SCTB specimen decreases with the increase of confining pressure.

The strengthening effect of the enhance layer on the mechanical properties of SCTB specimens is corroborated by

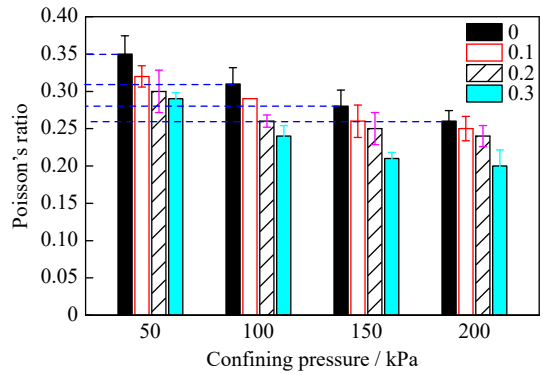

Fig. 12. Poisson's ratios of SCTB specimens with different thickness ratios of enhance layer.

the SEM micrographs and MIP analysis, which are conducted on the enhance layer of SCTB and CTB cured for 28 d before the triaxial compression test, as depicted in Fig. 13 and Fig. 14. It can be observed form Fig. 13 that the tailings particles in the enhance layer are covered with a higher presence of hydration products. After 28 d of hydration reaction, the hydration products predominantly manifest in the form of aggregates and lumps. The particles are tightly bonded by hydration products. As the quantity of hydration products increases, the number of pores gradually diminishes, resulting in a more compact internal structure in the enhance layer. Consequently, comparative analysis of SEM micrographs reveals that enhance layer has more hydration products and finer pore structure than CTB, which is conducive to improving the mechanical properties of SCTB specimens.

Fig. 14 illustrates the quantitative variation in the pore size distribution and pore volume distribution for CTB specimen and the enhance layer in SCTB. It can be observed from Fig. 14(a) that the CTB specimen has a more abundant and uneven pore structure, and is more likely to have large pores. In Fig. 14(b), it can be seen that the pore volume distribution curve of the CTB specimen consistently lies above that of the enhance layer in SCTB, which similarly indicates that the enhance layer has finer pore sizes. Additionally, the CTB specimen has a total porosity of 50.99%, whereas the enhance layer in SCTB has a lower total porosity of 40.62%. The results of SEM micrographs and MIP analysis indicate that the enhance layer in SCTB has a better pore structure and more hydration products, which results in superior compressive strength and elastic modulus compared to the upper and lower layers. Consequently, with an increase in the thickness ratio of the enhance layer, the proportion of high-strength layers within the SCTB samples also increases, leading to an enhancement in the overall mechanical property.

3.3. Energy dissipation evolution analysis

Adding the enhance layer can intensely alter the stress–strain response of SCTB specimens under triaxial compression. Indeed, the enhance layer will affect the energies stored or released evolution law of SCTB in the process of deformation and destruction stages as well. As obtained from many references, there are mainly four types of energy conversion among externally input energy, accumulated

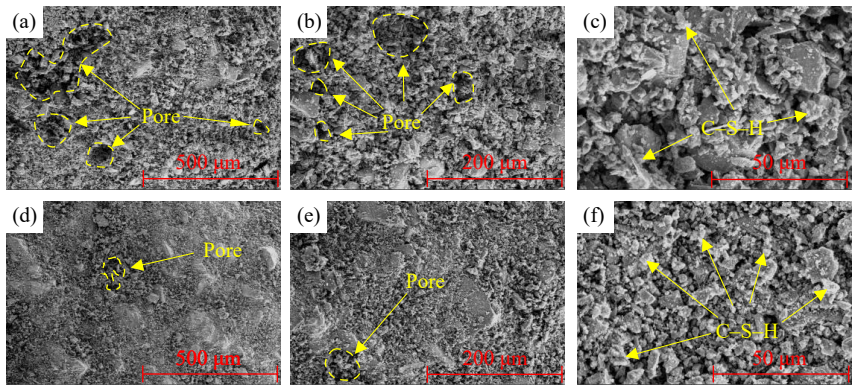

Fig. 13. SEM micrographs of CTB specimen (a–c) and the enhance layer of SCTB (d–f).

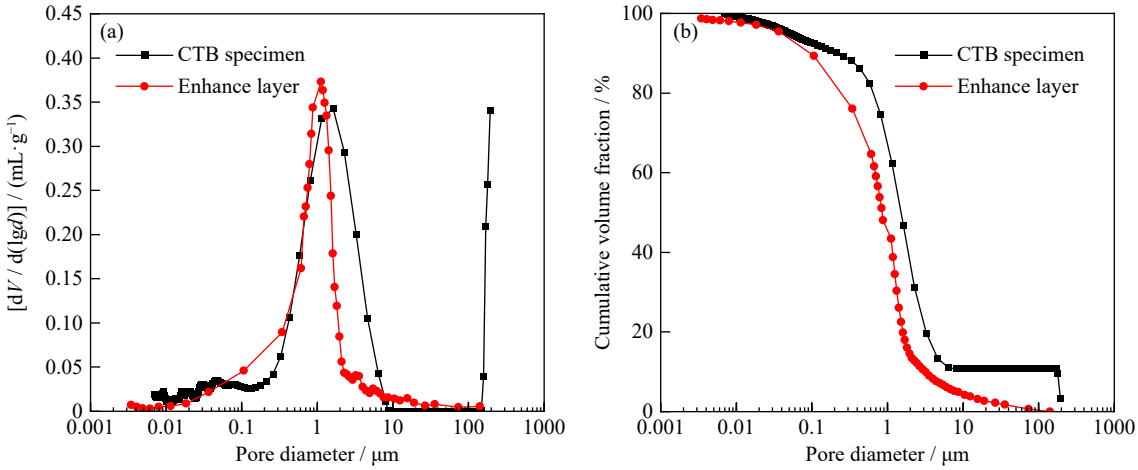

Fig. 14. Pore size distribution (a) and cumulative volume fraction (b) of CTB specimen and the enhance layer in SCTB.

elastic energy, dissipative energy, and released energy in the process of deformation and destruction stages of backfill [46–48]. The total energy and the elastic energy of the backfill in the three-dimensional stress state can be expressed as follows [49]:

$$U = U^{\mathrm{e}} + U^{\mathrm{d}} \tag{1}$$

$$U = \int_0^{\varepsilon_1} \sigma_1 \mathrm{d}\varepsilon_1 + 2\int_0^{\varepsilon_3} \sigma_3 \mathrm{d}\varepsilon_3 \tag{2}$$

$$U^{\mathrm{e}} = \frac{1}{2}\sigma_1\varepsilon_1^{\mathrm{e}} + \frac{1}{2}\sigma_2\varepsilon_2^{\mathrm{e}} + \frac{1}{2}\sigma_3\varepsilon_3^{\mathrm{e}} \tag{3}$$

For triaxial compression tests, the formula (3) of elastic energy can be simplified as:

$$U^{\mathrm{e}} = \frac{\sigma_1^2}{2E_0} + \frac{\sigma_3^2}{E_0} - \frac{\mu(2\sigma_1\sigma_3 + \sigma_3^2)}{E_0} \tag{4}$$

where U is the total energy, U^{d} is the dissipative energy, U^{e} is the elastic energy, σ_i and $\varepsilon_i^{\mathrm{e}}$ (i = 1, 2, 3) are the main stresses and the strain in the direction of the main stress, respectively, E_0 is the elastic modulus of the backfill, μ is the Poisson's ratio.

Six SCTB specimens with different thickness ratios (with fixed enhance layer position of 1/2) and positions (with fixed thickness ratio of 0.2) of enhance layer are selected for analysis, as shown in Fig. 15. The energy dissipation evolution process of SCTB specimens can be divided into four stages as shown in Fig. 15(d). They are: (I) Void closing stage: at the early phase of triaxial loading, the energy input by the external load is mainly used to compact interlaminar voids and close internal grain structures. (II) Elastic energy accumulation stage: as the loading progresses, most of the external input energy is converted into elastic energy and stored in the SCTB specimens. The elastic energy begins to accumulate rapidly, while the dissipative energy remains largely unchanged. (III) Dissipative energy growth stage: as the sample continues to be loaded, the plastic deformation occurs, the accumulation of elastic properties slows down, and the dissipative energy increases rapidly. (IV) Elastic energy release stage: when the applied load reaches and exceeds the peak strength of the SCTB specimen, the elastic energy reaches the maximum and begins to release, the growth rate of the dissipative energy increases, and the internal damage of the sample intensifies.

Fig. 16 illustrates the effect of the thickness ratio and the enhance layer position on the elastic energy of SCTB specimen. The elastic energy versus axial strain curves delineate the four distinct phases of progression. As shown in Fig. 16(a), the increase in the thickness ratio of the enhance layer shortens the strain process from accumulation of elastic energy to release. When the thickness ratio of the enhance layer is 0.3, the accumulated elastic energy is quickly released after the external load exceeds the peak compressive strength of the SCTB specimen, and the damage accumulates rapidly. This is also corroborated by the results from SEM micrographs and MIP analysis. The increased generation of hydra-

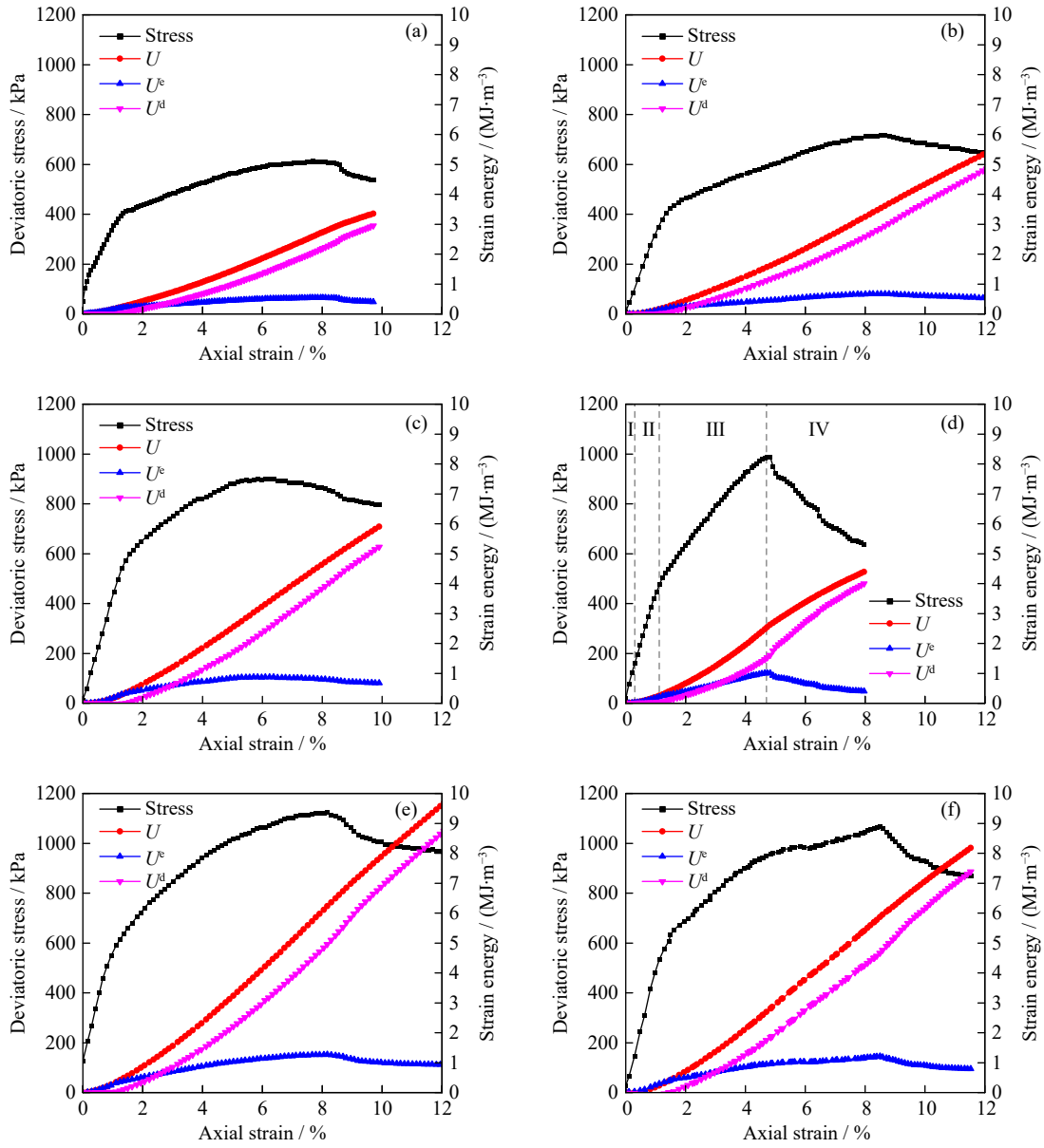

Fig. 15. Energy evolution of CTB and SCTB samples with different thickness ratios and positions of enhance layer under confining pressure of 100 kPa: (a) CTB without enhance layer; (b) thickness ratio of 0.1; (c) thickness ratio of 0.2; (d) thickness ratio of 0.3; (e) enhance layer position of 1/3; (f) enhance layer position of 2/3.

tion products not only fills the inter-particle pores but also enhances the cohesion and elastic modulus of SCTB sample. Consequently, as the thickness ratio of the enhance layer increases, the plastic deformation of the SCTB sample is reduced, and the elastic energy is increased. As shown in Fig. 16(b), the elastic stress curves of SCTB specimens with enhance layers at the position of 1/3 and 2/3 are similar and higher than those at the position of 1/2, which is consistent with the patterns observed in the stress–strain curves.

Fig. 17 shows the energy storage limit of SCTB specimens with different thickness ratios and positions of enhance layers under 100 kPa. As the thickness ratio of the enhance layer increases from 0 to 0.1, 0.2, and 0.3, the elastic energy rises from 0.54 to 0.67, 0.84 and 1.00 MJ·m^{-3}, representing a significant increase of 24.1%, 55.6% and 85.2%. As the position of enhance layer rises from 0 to 1/3, 1/2, and 2/3, the elastic energy rises from 0.54 to 1.24, 0.84 and 1.21 MJ·m^{-3}, representing a significant increase of 129.6%, 55.6% and 124.1%, respectively. The energy storage limit increases with the increase of enhance layer thickness ratio. The energy storage limit of the SCTB specimen with an enhance layer at the position of 1/2 is smaller than that at the position of 1/3 and 2/3, but still higher than that of the CTB specimen.

The energy storage limit is lowest when the enhance layer is positioned at 1/2 height compared to 1/3 and 2/3 due to the unique stress distribution and crack propagation characteristics in the specimen. When the enhance layer is placed at the position of 1/2, it coincides with the region where the maximum tensile stress occurs during the triaxial compression test. This alignment results in a higher stress concentration at the interface between the enhance layer and the surrounding weaker layers. The enhance layer, while providing some strength improvement, is not sufficient to fully counteract the high tensile stress in this critical region. Consequently, cracks

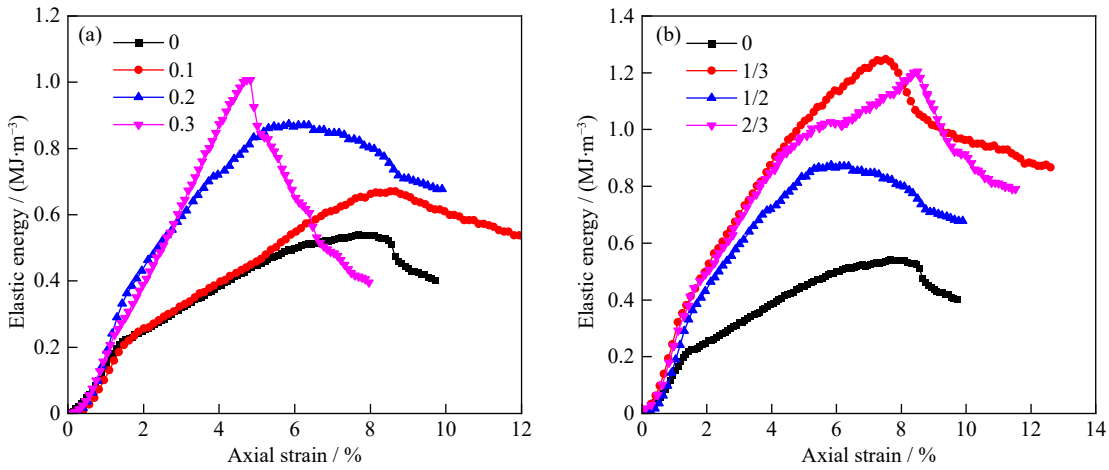

Fig. 16. Elastic energies of CTB and SCTB specimens with different thickness ratios (a) and positions of enhance layers (b) under confining pressure of 100 kPa.

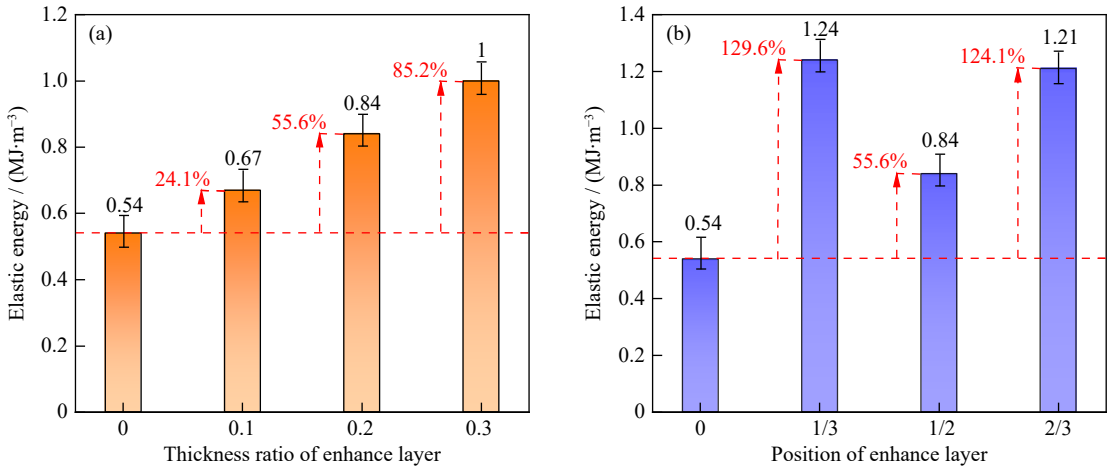

Fig. 17. Energy storage limits of CTB and SCTB specimens with different thickness ratios (a) and positions of enhance layers (b) under confining pressure of 100 kPa.

are more likely to penetrate the enhance layer, leading to premature failure of the specimen and thus a lower energy storage limit. In contrast, when the enhance layer is positioned at 1/3 or 2/3, it is located closer to the upper or lower of the specimen, where the tensile stress is relatively lower. The enhance layer in these positions can more effectively distribute the stress and provide additional strength to the weaker layers, delaying the onset of crack initiation and propagation. As a result, the specimen can withstand higher loads before failure occurs, leading to a higher energy storage limit compared to the 1/2 position. This conclusion is also supported by the peak strain and failure mode of the SCTB specimens. The prevailing belief is that an elevated energy storage limit can effectively impede the formation and propagation of cracks within the specimen. Therefore, the SCTB specimens exhibit better mechanical properties than the CTB, regardless of the thickness ratio and position of the enhance layer.

Fig. 18 presents the effects of enhance layer thickness ratio and position on the dissipative energy of the SCTB specimens. Unlike the elastic energy curve, the dissipative energy curves fail to distinctly discern the transition points between the four stages. The dissipative energy curves had no distinct differentiation between the void closing stage and elastic energy accumulation stage, and similarly, there is no distinct differentiation between the dissipative energy growth stage and elastic energy release stage. The dissipative energy curves of CTB specimens are consistently below SCTB specimens. It is generally accepted that a higher dissipative energy curve indicates a more rapid rate of specimen destruction. However, for SCTB specimens, the increase in dissipative energy is primarily attributed to the generation and propagation of cracks in the low-strength regions during the loading process, and the overall sample has not been destroyed.

3.4. Failure modes

Fig. 19 shows the failure modes of SCTB specimens with different enhance layer positions under different confining pressures. There is a big difference between SCTB and CTB, and the effect of enhance layer position on the failure pattern is dramatically diverse. The four main kinds of failure patterns are observed in the SCTB specimens, such as shear failure, shear bulging failure, splitting bulging failure, and hybrid failure. The shear failure is characterized by a shear plane, and the shear bulging failure is mainly manifested by a shear plane and bulging deformation. The splitting bulging

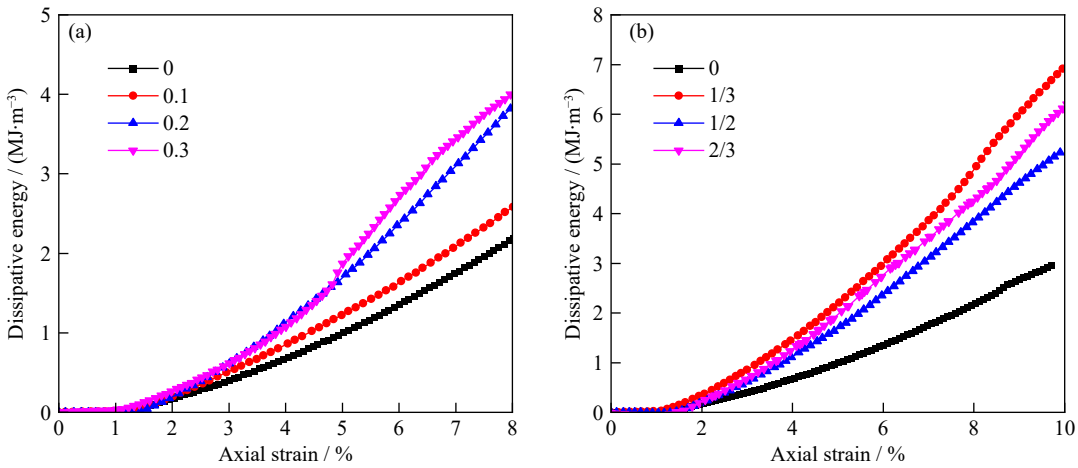

Fig. 18. Dissipative energy of CTB and SCTB specimens with different thickness ratios (a) and positions of enhance layers (b) under confining pressure of 100 kPa.

failure is dominated by vertical split cracks and lateral expansion deformation. The failure mode of CTB samples without enhance layer is shown in Fig. 19(a). The failure modes of CTB specimens are mainly manifested as shear failure through the whole specimen. With the increase of confining pressure, the failure mode slightly changes into shear bulging failure. In comparison with the CTB specimens, the SCTB specimens are obviously characterized by shear bulging failure and splitting bulging failure. For example, as shown in Fig 19(b), the SCTB specimen with an enhance layer thickness ratio of 0.2 and a position of 1/3 exhibits tensile failure in the upper layer when the confining pressure is 0 kPa. At low confining pressure (50 and 100 kPa), the splitting failure pattern occurs in SCTB with multiple critical cracks perpendicular to the enhance layer, as the confining pressure rises to 150 and 200 kPa, a zigzag shear banding extends along a plane from upper layer down to lower layer with a bulging deformation. In addition, the split cracks propagation path is mainly blocked by the enhance layer, and the split cracks are mainly generated at the upper layer or low layer, as shown in Fig 19(b) and Fig 19(d), this is mainly attributed to the stiffness effect induced by the enhance layer. The results also prove that the mechanical strength of SCTB with different enhance layer positions is higher than the CTB as obtained above.

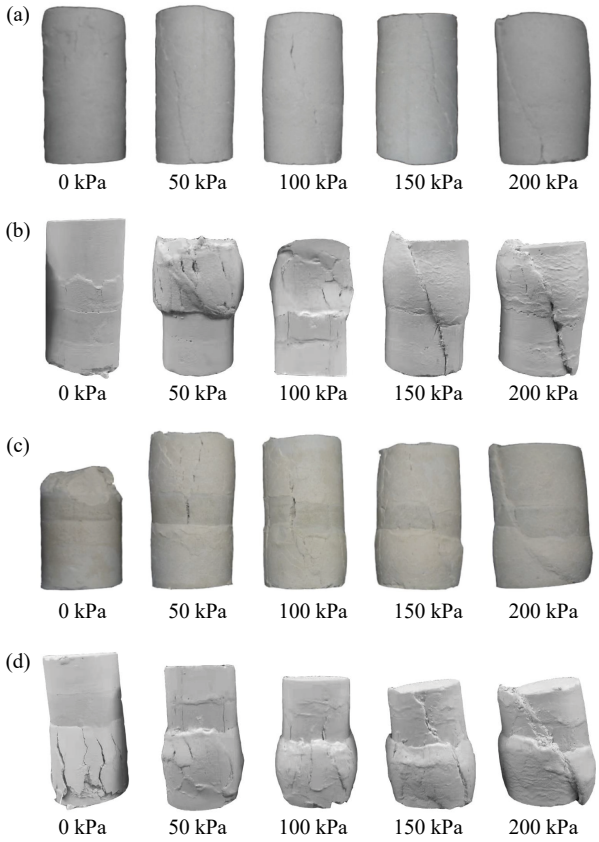

Fig. 19. Failure modes of SCTB specimens with different enhance layer positions: (a) CTB without enhance layer; (b) enhance layer position of 1/3; (c) enhance layer position of 1/2; (d) enhance layer position of 2/3.

Fig. 20 shows the effect of enhance layer thickness ratios (0.1, 0.2, and 0.3) on failure modes of SCTB specimens under triaxial compression. It can be observed that the splitting bulging failure at low confining pressure (0, 50, and 100 kPa)

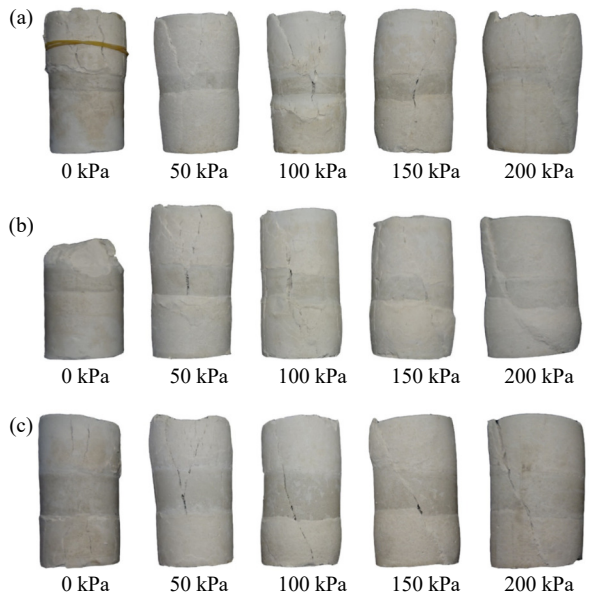

Fig. 20. Failure modes of SCTB specimens with different enhance layer thickness ratios: (a) 0.1; (b) 0.2; (c) 0.3.

and shear bulging failure under high confining pressure (150 and 200 kPa). The splitting cracks mainly initiate in the upper and lower layers and propagate until the enhance layer. However, the crack propagation is mostly blocked by the enhance layer, only a few cracks penetrate through the enhance layer. The thicker the enhance layer is, the more obvious the block isolation effect is. Namely, as the thickness ratio of the enhance layer increases, it becomes more difficult for cracks to penetrate through the enhance layer, thereby enhancing the strength of SCTB.

4. Conclusions

The effect of the enhance layer on the triaxial compressive mechanical properties of SCTB in open stoping mines was investigated. The stress–strain curves, strength features, energy evolution, failure patterns, and microstructures of SCTB with different enhance layer positions and thickness ratios were analyzed by triaxial compression tests and SEM–MIP tests. The following inferences could be summarized from the above results.

(1) The incorporation of an enhance layer has a strengthening effect on SCTB's deformation response, peak strength, and failure pattern. As the confining pressure increases, the slopes of the curves in the elastic stage become steeper, and the peak deviatoric stresses and axial strains at failure of the SCTB specimens increase as well, irrespectively of enhance layer position and thickness ratio. Moreover, the plastic phase of SCTB is extended accordingly compared with the SCTB without enhance layer.

(2) The Poisson's ratios of the SCTB specimens with different enhance layer positions and thickness ratios decrease with the increase of confining pressure. The internal friction angles and cohesions of the SCTB specimens are higher than those of the CTB specimens, however, the cohesion is more susceptible to enhance layer position and thickness ratio than the internal friction angle.

(3) The effect of incorporating an enhance layer is particularly evident during the elastic-plastic phase. The incorporation of enhance layer greatly prolongs the plastic steps, and the accumulation of energy will rise rapidly at this stage. Therefore, high energy storage in SCTB will lead to a rapid stress fall and energy release after the backfill peak.

(4) The SCTB's failure patterns are shear failure, shear bulging failure, splitting bulging failure, and hybrid failure. The failure style of SCTB specimens changed from shear failure to splitting bulging failure and shear bulging failure with enhance layer adding. The crack propagation path was significantly blocked by the enhance layer.

(5) Unlike the traditional method of enhancing the strength and stability of SCTB by increasing the cement-to-tailings ratio in the middle layer, this study introduces a new method for enhancing the strength of SCTB. This method can optimize the filling parameters and SCTB structures, achieving or exceeding the strength and stability requirements of mines while reducing filling costs and carbon emissions, which has a good application prospect.

The results of the study show that CTB with enhance layer structure had good strength response features and could be employed in subsequent stoping backfilling mines. In subsequent research, conducting long-term stability studies under various environmental conditions, such as different temperatures and humidity levels, would provide insights into the durability of SCTB over time. This is particularly important for applications where SCTB is used in large-scale mining operations. Moreover, developing more sophisticated numerical models to simulate the behavior of SCTB under different loading conditions and environmental factors could complement experimental studies. This would help in predicting the performance of SCTB in real-world scenarios and guide the design of more effective backfilling strategies.

Acknowledgements

This work was financially supported by the Fundamental Research Funds for the Central Universities (No. 2023JCCXNY01) and Guangxi Key Technologies R&D Program (No. 2022AB31022).

Conflict of Interest

The authors declare that there is no conflict of interest.

References

[1] L.H. Yang, H.W. Jia, A.X. Wu, *et al*., Particle aggregation and breakage kinetics in cemented paste backfill, *Int. J. Miner. Metall. Mater.*, 31(2024), No. 9, p. 1965.

[2] L. Yang, W.B. Xu, E. Yilmaz, Q. Wang, and J.P. Qiu, A combined experimental and numerical study on the triaxial and dynamic compression behavior of cemented tailings backfill, *Eng. Struct.*, 219(2020), art. No. 110957.

[3] J.R. Zhou, J.F. Lou, J. Wei, F. Dai, J.K. Chen, and M.S. Zhang, A 3D microseismic data-driven damage model for jointed rock mass under hydro-mechanical coupling conditions and its application, *J. Rock Mech. Geotech. Eng.*, 15(2023), No. 4, p. 911.

[4] D.F. Zhao, S.Y. Zhang, and Y.L. Zhao, Recycling arsenic-containing bio-leaching residue after thermal treatment in cemented paste backfill: Structure modification, binder properties and environmental assessment, *Int. J. Miner. Metall. Mater.*, 31(2024), No. 10, p. 2136.

[5] S.V. Chmykhalova, Toward a reclamation effort estimation procedure for open pit mines, *Eurasian Min*., (2023), No. 1, p. 83.

[6] K. Fang and L. Cui, Experimental investigation of fiber content and length on curing time-dependent mode-I fracture behavior and properties of cemented paste backfill and implication to engineering design, *Fatigue Fract. Eng. Mater. Struct.*, 45(2022), No. 11, p. 3302.

[7] X. Nan, X.X. Liu, B.Q. Wu, H.M. Zhang, K.J. Song, and X.D. Wang, Coupled CFD-DEM simulation and experimental study of particle distribution and accumulation during tailings seepage process, *J. Cleaner Prod.*, 427(2023), art. No. 139229.

[8] C.C. Qi, A. Fourie, and Q.S. Chen, Neural network and particle swarm optimization for predicting the unconfined compressive strength of cemented paste backfill, *Constr. Build. Mater.*, 159(2018), p. 473.

[9] M.G. Shannon, Reliability assessment of an open pit slope on

bong iron ore mine, *J. Geosci. Environ. Prot.*, 9(2021), No. 3, p. 31.
[10] W. Chen, S.H. Yin, G.M. Zhou, Z.K. Li, and Q. Song, Copper recovery from tailings through bioleaching and further application of bioleached tailings residue: Comprehensive utilization of tailings, *J. Cleaner Prod.*, 332(2022), art. No. 130129.
[11] W.B. Xu, Q.L. Li, and Y.L. Zhang, Influence of temperature on compressive strength, microstructure properties and failure pattern of fiber-reinforced cemented tailings backfill, *Constr. Build. Mater.*, 222(2019), p. 776.
[12] W.B. Xu, Y.L. Zhang, and B. Liu, Influence of silica fume and low curing temperature on mechanical property of cemented paste backfill, *Constr. Build. Mater.*, 254(2020), art. No. 119305.
[13] A.B. Jin, J. Wang, S.J. Chen, and H. Li, Strength and damage characteristics of tailings filling body with different particle size distributions, *Rock Soil Mech.*, 43(2022), No. 11, p. 3083.
[14] M. Jssem and N.M. Fawzi, Effect of expanded perlite aggregate and silica fume on some properties of lightweight concrete, *J. Eng.*, 30(2024), No. 5, p. 172.
[15] W.B. Xu, Y.L. Zhang, X.H. Zuo, and M. Hong, Time-dependent rheological and mechanical properties of silica fume modified cemented tailings backfill in low temperature environment, *Cem. Concr. Compos.*, 114(2020), art. No. 103804.
[16] H. Qin, S. Cao, and E. Yilmaz, Mechanical, energy evolution, damage and microstructural behavior of cemented tailings-rock fill considering rock content and size effects, *Constr. Build. Mater.*, 411(2024), art. No. 134449.
[17] Q.S. Chen, Q.L. Zhang, C.C. Qi, A. Fourie, and C.C. Xiao, Recycling phosphogypsum and construction demolition waste for cemented paste backfill and its environmental impact, *J. Cleaner Prod*., 186(2018), p. 418.
[18] H. Lin, R.S. Yang, Y.L. Li, S.Z. Fang, Z.Y. Tan, and H. Ni, Mechanical properties and fracture evolution of layered gangue-cemented backfill, *Min. Metall. Explor.*, 41(2024), No. 6, p. 3119.
[19] N.M. Chiloane, F. Sengani, and F. Mulenga, An experimental and numerical study of the strength development of layered cemented tailings backfill, *Sci. Rep.*, 14(2024), No. 1, art. No. 734.
[20] X.B. Qin, P. Wang, L. Liu, M. Wang, and J. Xin, Sensitivity analysis of microstructure parameters and mechanical strength during consolidation of cemented paste backfill, *Math. Probl. Eng.*, 2018(2018), art. No. 5170721.
[21] A. Ghirian and M. Fall, Strength evolution and deformation behaviour of cemented paste backfill at early ages: Effect of curing stress, filling strategy and drainage, *Int. J. Min. Sci. Technol.*, 26(2016), No. 5, p. 809.
[22] J. Wang, J.X. Fu, W.D. Song, Y.F. Zhang, and Y. Wang, Mechanical behavior, acoustic emission properties and damage evolution of cemented paste backfill considering structural feature, *Constr. Build. Mater.*, 261(2020), art. No. 119958.
[23] C. Zhang, J.X. Fu, W.D. Song, M.C. Kang, T. Li, and N.W. Wang, Analysis on mechanical behavior and failure characteristics of layered cemented paste backfill(LCPB) under triaxial compression, *Constr. Build. Mater.*, 324(2022), art. No. 126631.
[24] B.W. Wang, L. Yang, Q.L. Li, X.Y. Shu, and M.C. Kang, Mechanical behavior, acoustic emission and principal strain field evolution properties of layered cemented paste backfill under unconfined compression, *Constr. Build. Mater.*, 415(2024), art. No. 135111.
[25] S. Cao, E. Yilmaz, and W.D. Song, Dynamic response of cement-tailings matrix composites under SHPB compression load, *Constr. Build. Mater.*, 186(2018), p. 892.
[26] S.J. Chen, A.B. Jin, Y.Q. Zhao, H. Li, and J. Wang, Mechanical properties and deformation mechanism of stratified cemented tailings backfill under unconfined compression, *Constr. Build. Mater.*, 335(2022), art. No. 127205.
[27] W.B. Xu, Y. Cao, and B.H. Liu, Strength efficiency evaluation of cemented tailings backfill with different stratified structures, *Eng. Struct.*, 180(2019), p. 18.
[28] H.Z. Jiao, W.X. Zhang, Y.F. Wang, X.M. Chen, L.H. Yang, and Y.Y. Rong, Study on strength reduction law and meso-crack evolution of lower layered cemented tailings backfill, *J. Renewable Mater.*, 11(2023), No.3, p. 1513.
[29] Z.Y. Li, W. Sun, T. Gao, J.G. Zhao, K.F. Lu, and H.Y. Cheng, Experimental study on evolution of pore structure of inclined layered cemented tailings backfill based on X-ray CT, *Constr. Build. Mater.*, 366(2023), art. No. 130242.
[30] H.J. Lu, Y.R. Wang, D.Q. Gan, J. Wu, and X.J. Wu, Numerical investigation of the mechanical behavior of the backfill−rock composite structure under triaxial compression, *Int. J. Miner. Metall. Mater.*, 30(2023), No. 5, p. 802.
[31] Z.H. Zhang and J.C. Li, Experimental investigation on strength and failure characteristics of cemented paste backfill, *Front. Mater.*, 8(2021), art. No. 792561.
[32] Z.B. Guo, J.P. Qiu, A. Kirichek, H. Zhou, C. Liu, and L. Yang, Recycling waste tyre polymer for production of fibre reinforced cemented tailings backfill in green mining, *Sci. Total Environ.*, 908(2024), art. No. 168320.
[33] X. Yu, J. Kemeny, Y.Y. Tan, W.D. Song, and K. Huang, Mechanical properties and fracturing of rock-backfill composite specimens under triaxial compression, *Constr. Build. Mater.*, 304(2021), art. No. 124577.
[34] J.J. Wang, D. Ma, J.W. Zhang, and Q. Li, Effect of wet-dry cycle on triaxial mechanical properties and constitutive models of solid waste cemented backfill, *Constr. Build. Mater.*, 435(2024), art. No. 136863.
[35] W.B. Xu, W.L. Wu, and B. Liu, Effect of curing age, cement content and confining pressure on the saturated hydraulic conductivity and triaxial compressive behavior of cemented tailings backfill, *J. Cent. South Univ.*, 30(2023), p. 1649.
[36] S. Wang, G.D. Mei, W.X. Wang, *et al*., Experimental study of triaxial shear features of concentrated full tailings considering the effect of curing age, *Front. Earth Sci.*, 11(2023), art. No. 1158715.
[37] ASTM International, ASTM D4767–11: *Standard Test Method for Consolidated Undrained Triaxial Compression Test for Cohesive Soils*, ASTM International, West Conshohocken, 2020.
[38] Q. Yin, F. Wen, Z.G. Tao, *et al*., Effects of aggregate size distribution and carbon nanotubes on the mechanical properties of cemented gangue backfill samples under true triaxial compression, *Int. J. Miner. Metall. Mater.*, 32(2025), No. 2, p. 311.
[39] S. Goodarzi and H. Shahnazari, Strength enhancement of geotextile-reinforced carbonate sand, *Geotext. Geomembr.*, 47(2019), No. 2, p. 128.
[40] W.B. Xu, B. Liu, and W.L. Wu, Strength and deformation behaviors of cemented tailings backfill under triaxial compression, *J. Cent. South Univ.*, 27(2020), p. 3531.
[41] W.L. Wu, W.B. Xu, and J.P. Zuo, Effect of inclined interface angle on shear strength and deformation response of cemented paste backfill-rock under triaxial compression, *Constr. Build. Mater.*, 279(2021), art. No. 122478.
[42] J.X. Fu, J. Wang, and W.D. Song, Damage constitutive model and strength criterion of cemented paste backfill based on layered effect considerations, *J. Mater. Res. Technol.*, 9(2020), No. 3, p. 6073.
[43] Z. Zhou, Z.Z. Liu, H. Yang, W.Y. Gao, and C.C. Zhang, Freeze-thaw damage mechanism of elastic modulus of soil-rock mixtures at different confining pressures, *J. Cent. South Univ.*, 27(2020), p. 554.
[44] T.Z. Zhang, H.G. Ji, X.B. Su, *et al*., Evaluation and classification of rock heterogeneity based on acoustic emission detection, *Int. J. Miner. Metall. Mater.*, 29(2022), No. 12, p. 2117.

[45] Z.G. Xiu, S.H. Wang, Y.C. Ji, F.L. Wang, and F.Y. Ren, Experimental study on the triaxial mechanical behaviors of the Cemented Paste Backfill: Effect of curing time, drainage conditions and curing temperature, *J. Environ. Manage.*, 301(2022), art. No. 113828.

[46] K. Zhao, Y. Zhou, S.H. Yin, *et al*., Effect of initial defects on the microstructure, mechanics, and energy dissipation characteristics of cemented paste backfill, *Mater. Today Commun.*, 35(2023), art. No. 105785.

[47] Y. Zhou, Y.J. Yan, K. Zhao, *et al*., Study of the effect of loading modes on the acoustic emission fractal and damage characteristics of cemented paste backfill, *Constr. Build. Mater.*, 277(2021), art. No. 122311.

[48] Y.Q. Hou, S.H. Yin, S.X. Yang, X. Chen, and H.H. Du, Mechanical properties, damage evolution and energy dissipation of cemented tailings backfill under impact loading, *J. Build. Eng.*, 66(2023), art. No. 105912.

[49] S. Luo, F.Q. Gong, L.L. Li, and K. Peng, Linear energy storage and dissipation laws and damage evolution characteristics of rock under triaxial cyclic compression with different confining pressures, *Trans. Nonferrous Met. Soc. China*, 33(2023), No. 7, p. 2168.